Science Advances
AAAS

Supplementary Materials for

Molecular mechanism of *S*-adenosylmethionine sensing by SAMTOR in mTORC1 signaling

Xin Tang *et al.*

Corresponding author: Jianping Ding, jpding@sibcb.ac.cn; Tianlong Zhang, tlzhang@shu.edu.cn

Sci. Adv. **8**, eabn3868 (2022)
DOI: 10.1126/sciadv.abn3868

This PDF file includes:

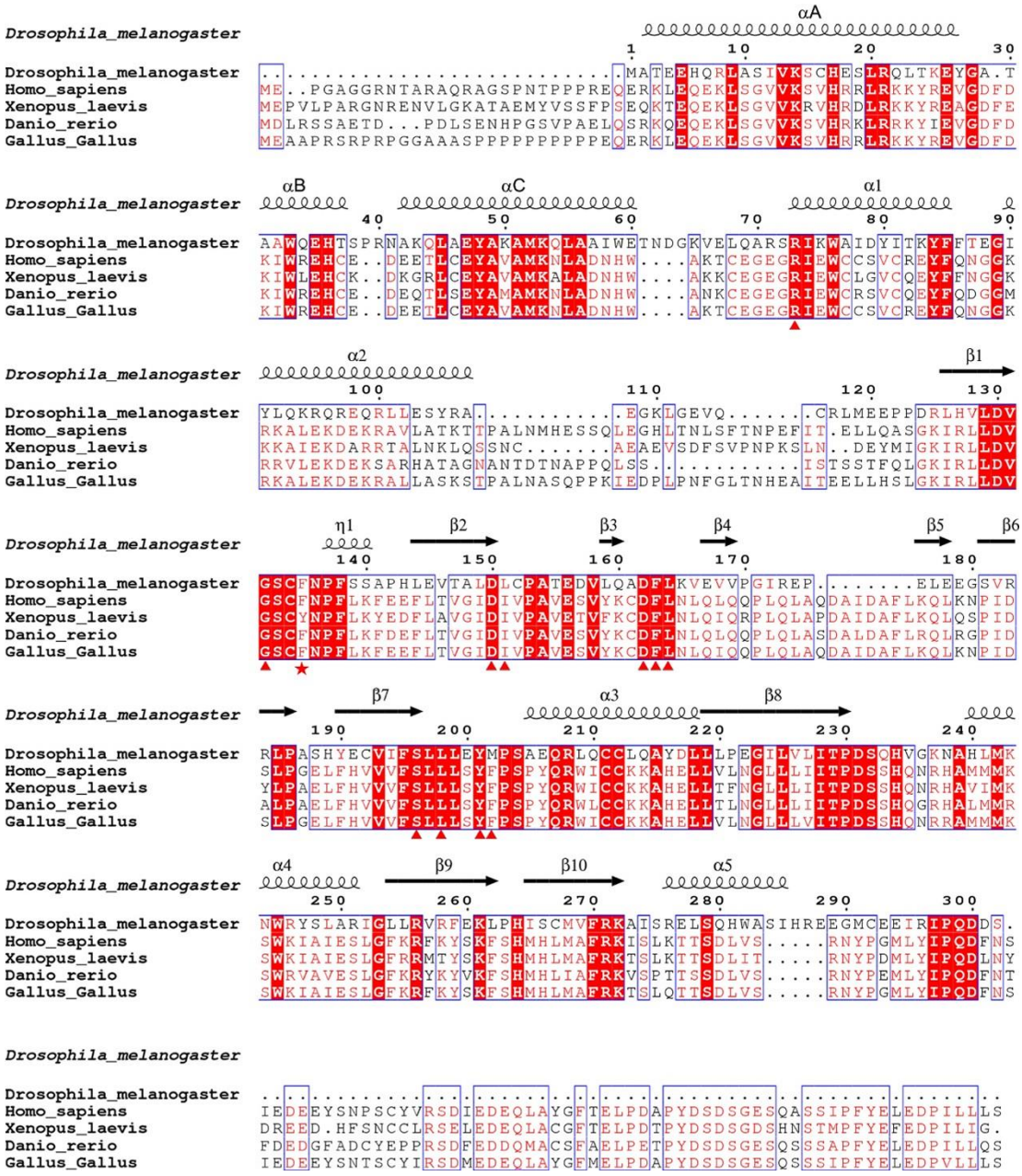

Figure S1. Sequence comparison of SAMTOR from several representative species. The secondary structure elements of dSAMTOR are placed on the top of the alignment. The residues involved in the ligand binding and the GATOR1-KICSTOR binding are indicated with triangle and star, respectively. The sequence alignment was performed using the program ESPript (*58*).

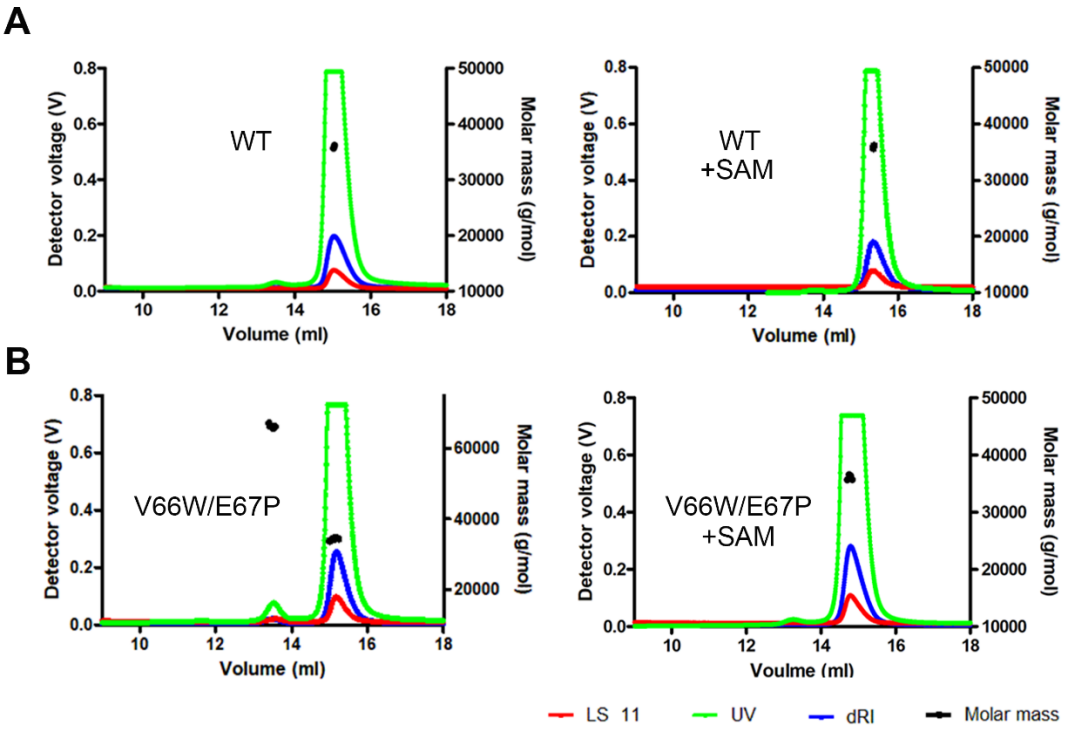

Figure S2. Size-exclusion chromatography coupled with multi-angle light scattering (SEC-MALS) analysis of dSAMTOR (10 mg/ml) in the absence and presence of SAM (1 mM). (**A**) The wild-type (WT) dSAMTOR. (**B**) The V66W/E67P mutant dSAMTOR. The SEC-MALS analyses were performed three times which yielded similar results, and for each case only the result of one representative experiment is shown.

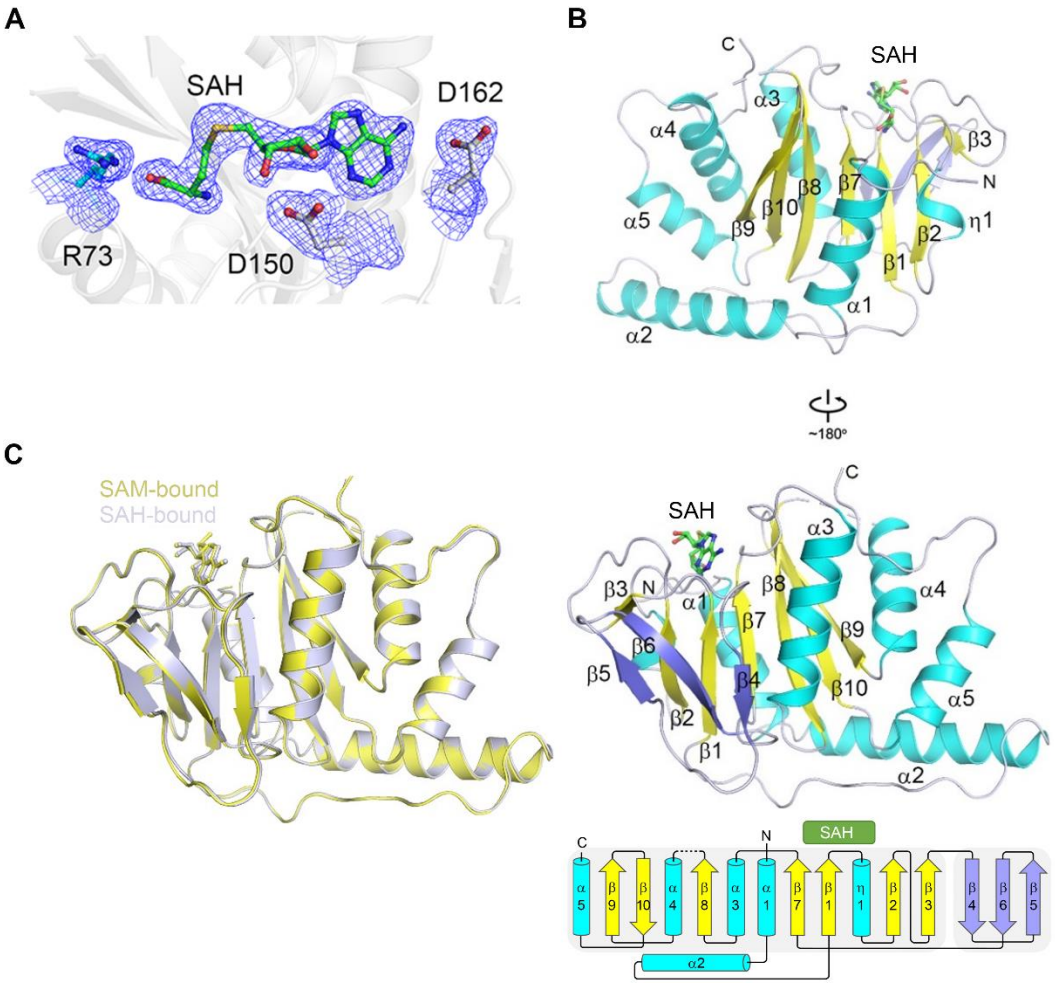

Figure S3. Crystal structure of the SAH-bound MTase domain of dSAMTOR. (**A**) Composite simulated annealing Fo-Fc omit map (contoured at 1.5 σ) for the bound SAH and several surrounding residues. (**B**) Overall structure of the SAH-bound MTase domain of dSAMTOR in two different views. The α-helices, major β-sheet and minor β-sheet are colored in cyan, yellow and blue, respectively. The bound SAH is shown with a stick model in green. The topology of the secondary structure elements of the MTase domain is shown below. The linker between β8 and α4 (residues 233-239) is disordered and thus is shown with a dashed line. (**C**) Superposition of the SAH-bound (light blue) and SAM-bound (yellow) MTase domain structures.

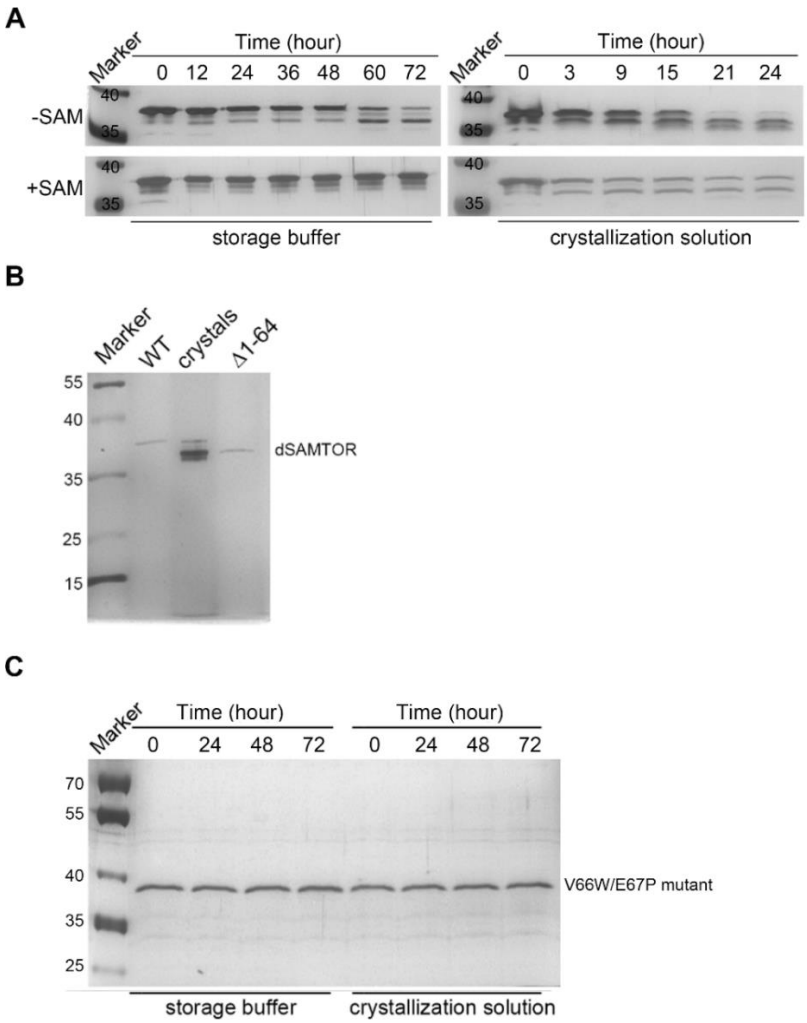

Figure S4. SDS-PAGE analysis of different dSAMTOR samples. (**A**) Stability analyses of the full-length wild-type (WT) dSAMTOR in the absence and presence of SAM (molar ratio of dSAMTOR:SAM = 1:3) in the storage buffer and the crystallization solution at indicated times. The SDS-PAGE analysis results were detected by silver staining. In the absence of SAM, the full-length dSAMTOR is unstable and the N-terminal region is gradually degraded in the storage buffer and the crystallization solution in a time-dependent manner. In the presence of SAM, the degradation of the full-length dSAMTOR is substantially alleviated but not completely prevented in both solutions. The full-length dSAMTOR was degraded more quickly in the crystallization solution than in the storage buffer. (**B**) SDS-PAGE analysis of the full-length WT dSAMTOR used in the crystallization (WT), the dissolved crystals of the SAM-bound MTase domain of dSAMTOR (crystals), and the Δ1-64 truncated dSAMTOR (Δ1-64). The N-terminal region of dSAMTOR was degraded in the crystals. (**C**) Stability analysis of the full-length V66W/E67P mutant dSAMTOR in the storage buffer and the crystallization solution at indicated times. The V66W/E67P mutant dSAMTOR was stable in both solutions. The SDS-PAGE analyses were performed at least three times except for the dissolved crystals of the SAM-bound MTase domain of dSAMTOR in (B) which was performed only once due to limited amount of the crystals. The repeated experiments yielded similar results and for each case, only the result of one representative experiment is shown.

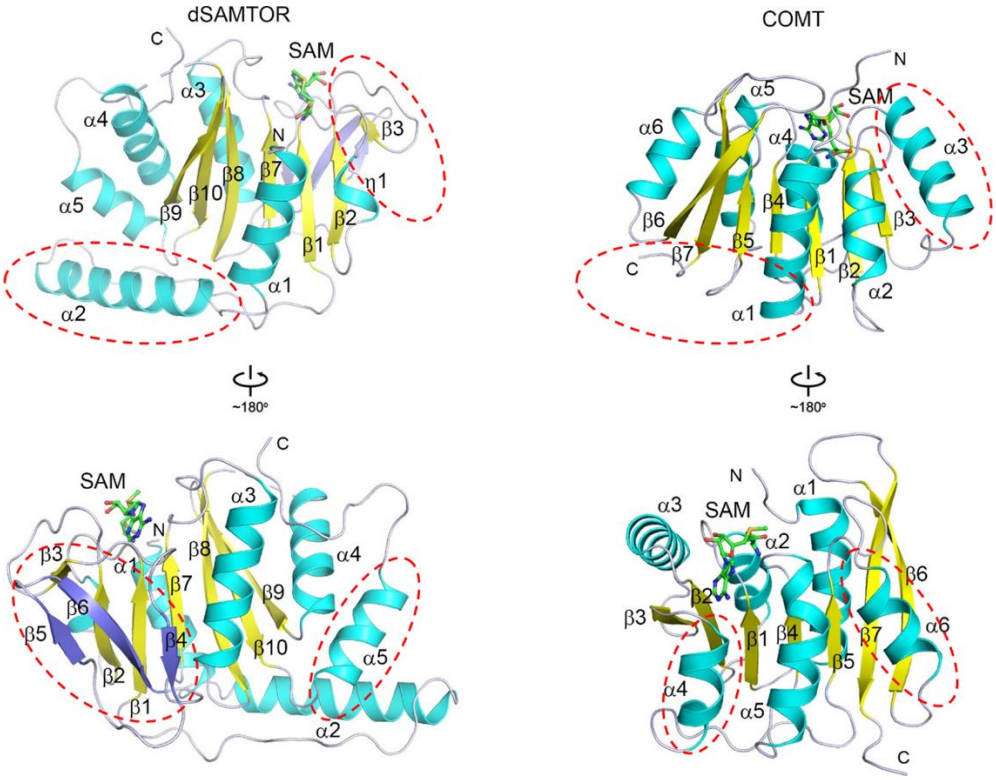

Figure S5. Structural comparison of the SAM-bound MTase domain of dSAMTOR and that of the catechol O-methyltransferase (COMT, PDB code 1VID) (*59*) which assumes a prototypical class I MTase fold (*25*). The cartoon representations of dSAMTOR are the same as in Figure 1C. The overall structures of COMT are shown in similar orientations as those of dSAMTOR. The α-helices and β-sheet are colored in cyan and yellow, respectively. The bound SAM is shown with a stick model in green. The major structural differences between dSAMTOR and COMT are indicated by dashed circles.

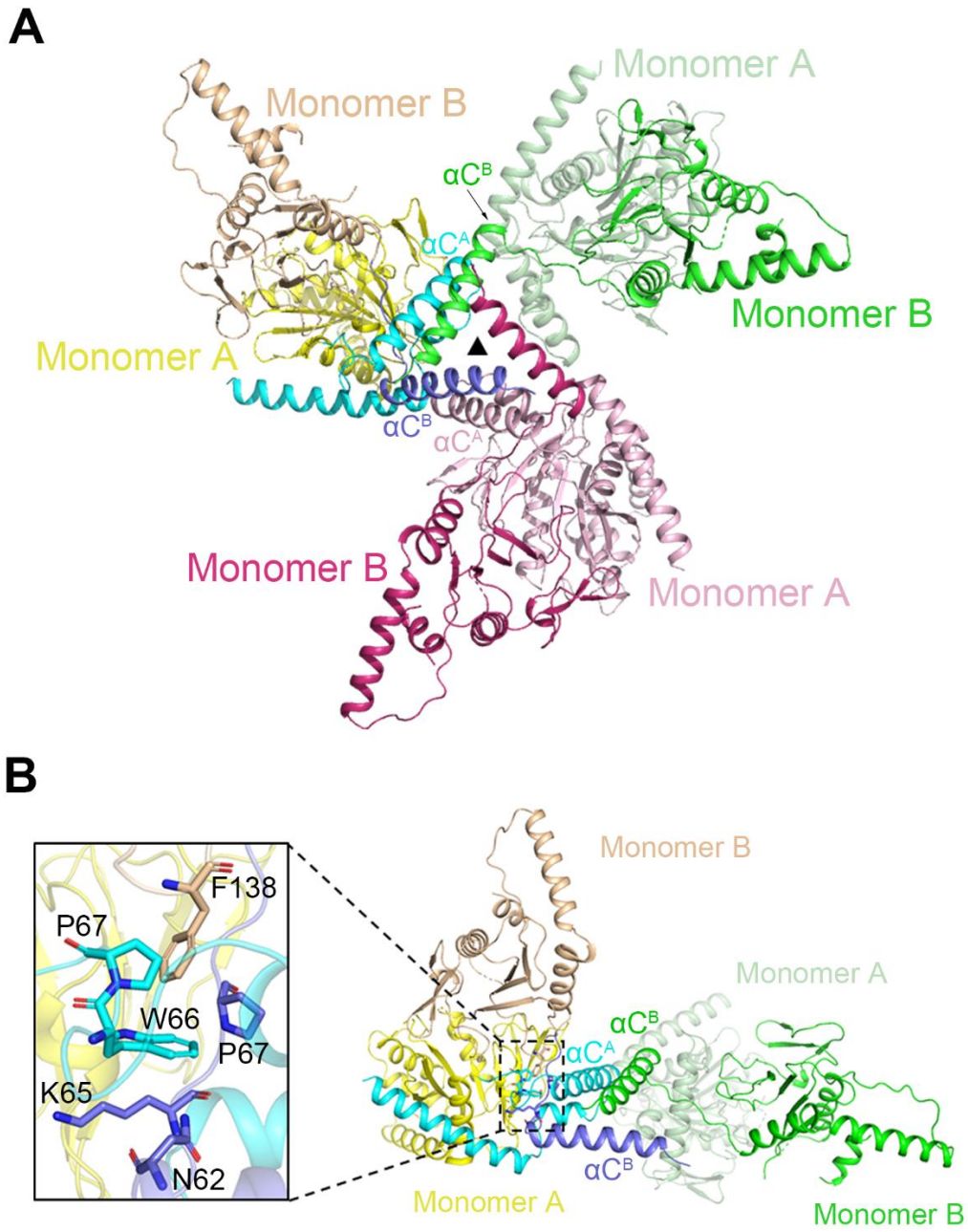

Figure S6. Crystal packing analysis of the apo V66W/E67P mutant dSAMTOR structure. **(A)** The αC helices of both monomers A and B participate in crystal packing and make contacts with these of three-fold axis-related monomers. The color coding scheme of dSAMTOR is the same as in **Figure 2B**. The three-fold axis-related monomers A and B are colored in light and dark green and light and dark pink, respectively. **(B)** The linker regions containing the V66W/E67P double mutation in the two monomers are crossed over and make interactions with each other but are not involved in crystal packing. The zoomed-in box shows the interactions between the linker regions of monomer A and monomer B.

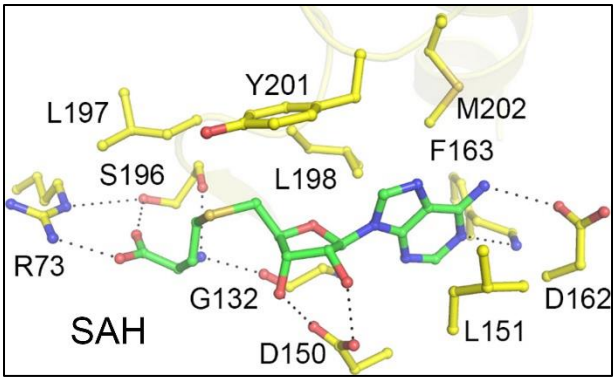

Figure S7. Interactions between SAH and the surrounding residues in the structure of the SAH-bound MTase domain of dSAMTOR. SAH is shown in green and the surrounding residues in yellow.

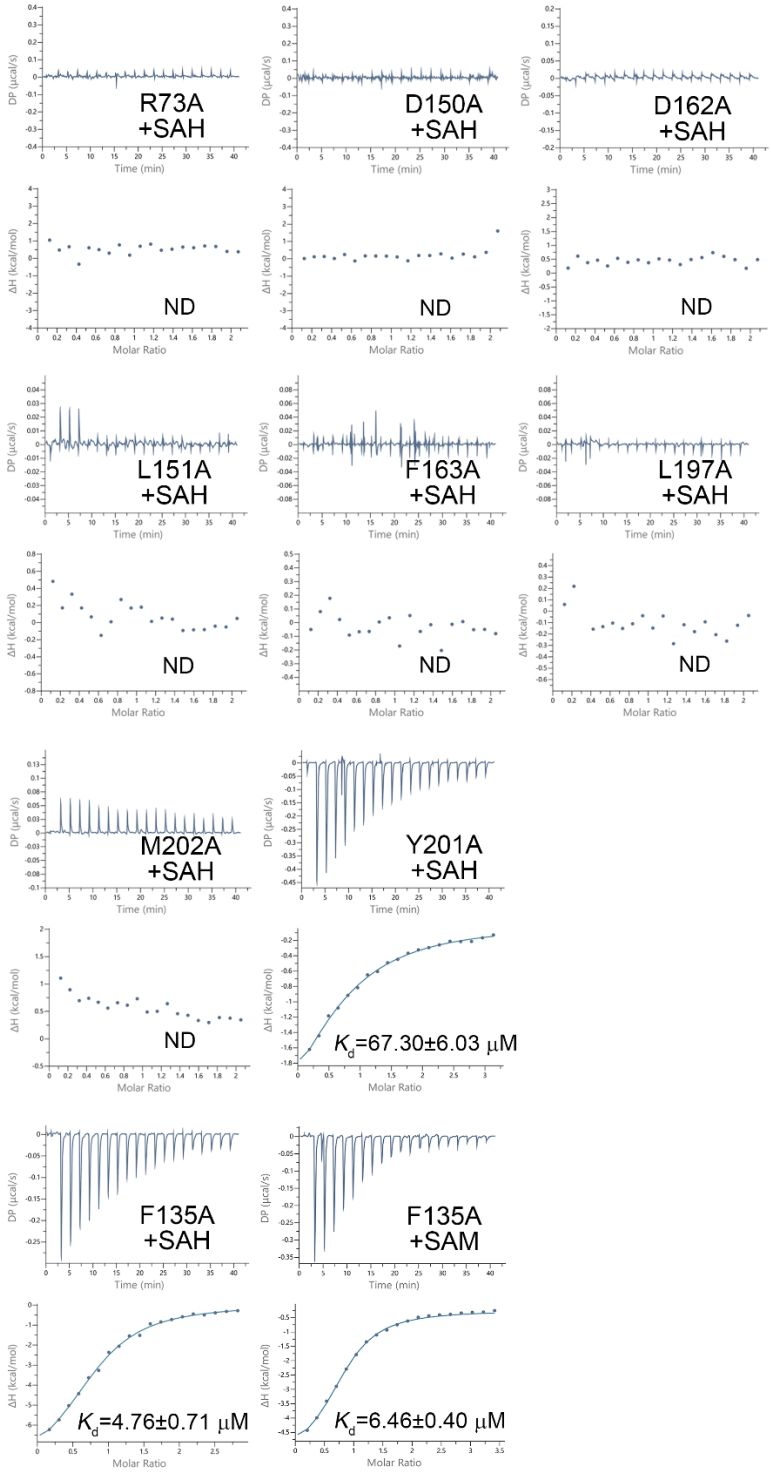

Figure S8. ITC measurements for the ligand-binding affinity of different dSAMTOR mutants. ND, not detected. The experiments were performed three times for those with measurable binding and two times for those with undetectable binding, and the repeated experiments yielded similar results; for each case, only the result of one representative experiment is shown.

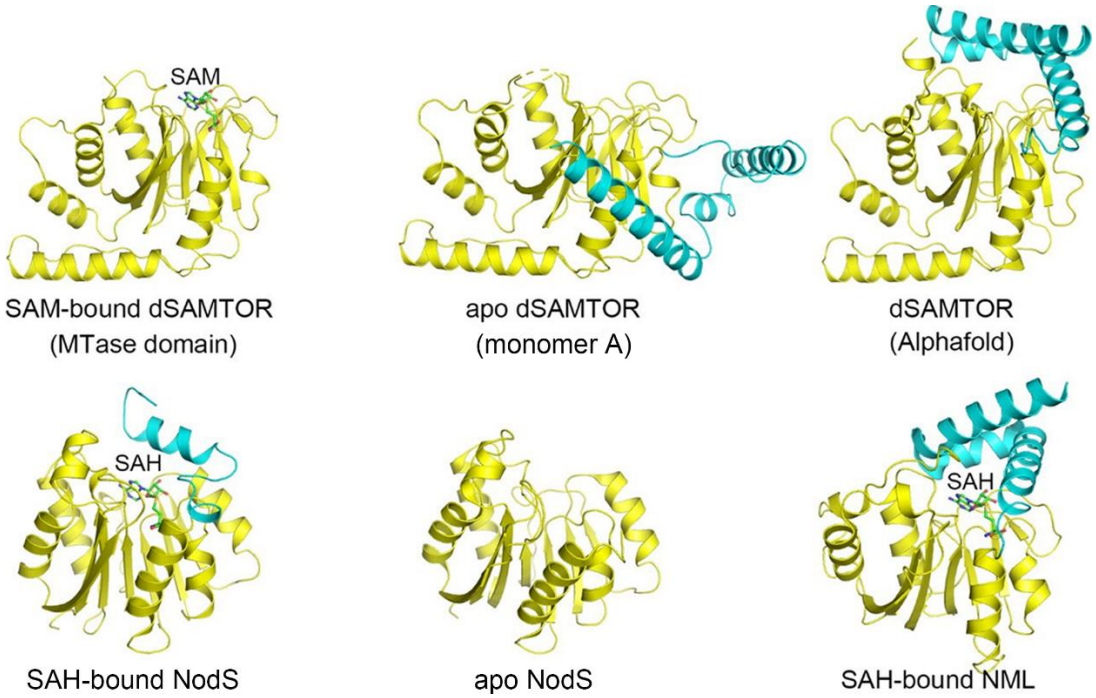

Figure S9. Structural comparison of different class I SAM-dependent MTases. Structural comparison of the SAM-bound MTase domain of dSAMTOR, the apo full-length V66W/E67P mutant dSAMTOR (monomer A), the AlphaFold predicted dSAMTOR structure (*33*), the SAH-bound and apo Nodulation protein S (NodS, PDB codes 3OFK and 3OFJ) (*30*), and the SAH-bound Nucleomethylin (NML, PDB code 2ZFU) (*29*). The MTase domains of different MTases are colored in yellow and viewed in similar orientations, and the N-terminal domains are colored in cyan. The bound ligand (SAM or SAH) is shown with stick model in green.

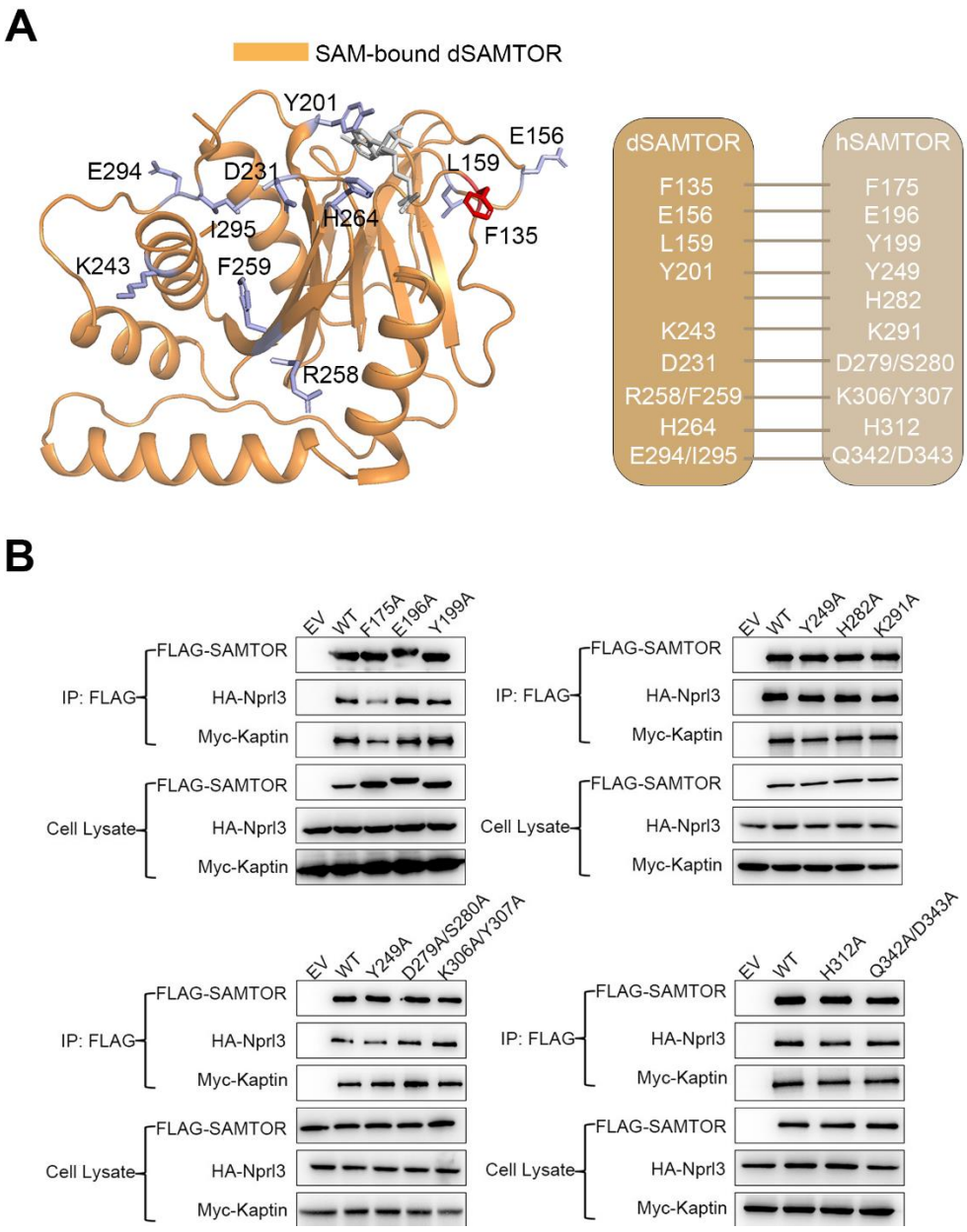

Figure S10. Co-immunoprecipitation (co-IP) assay to examine the interactions of the wild-type (WT) and hSAMTOR mutants with HA-Nprl3 and Myc-Kaptin in HEK 293T cells. **(A)** Spatial positions of some conserved residues near the ligand-binding site and on the solvent exposed surface of the SAM-bound dSAMTOR MTase domain. The equivalent residues of hSAMTOR are mutated in the co-IP assay. The correspondence of the residues between dSAMTOR and hSAMTOR is shown on the right panel. **(B)** Co-IP assay to examine the interactions of the wild-type (WT) and hSAMTOR mutants with HA-Nprl3 and Myc-Kaptin in HEK 293T cells. Among the tested mutants, only the F175A hSAMTOR mutant exhibits a substantially decreased binding with GATOR1-KICSTOR. The assays were performed three times which yielded similar results, and for each case only the result of one representative experiment is shown.

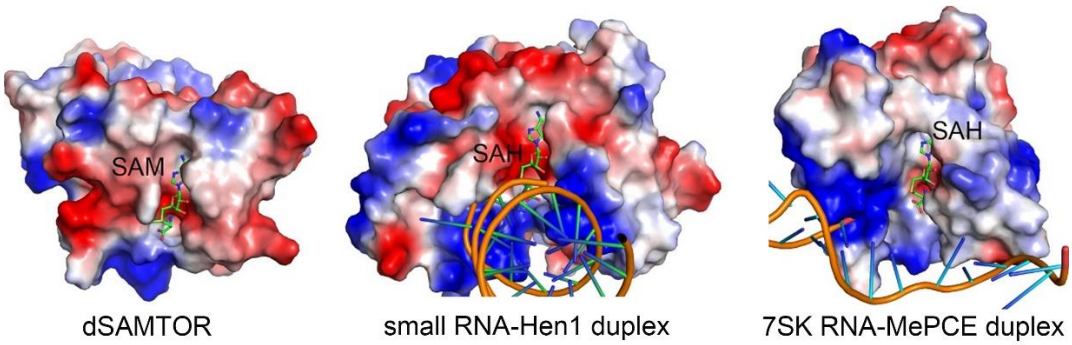

Figure S11. Comparison of the electrostatic surfaces of the SAM-bound MTase domains of dSAMTOR, the RNA MTase Hen1 in complex with a small RNA duplex (PDB code 3HTX) (*48*), and the RNA MTase MePCE in complex with a long noncoding RNA duplex (PDB code 6DCB) (*49*). Both HenI and MePCE belong to the class I MTases. The proteins are shown with electrostatic surfaces; the bound ligands are shown with stick models; and the bound RNAs are shown with ribbon models.

REFERENCES AND NOTES

1. M. Cornu, V. Albert, M. N. Hall, mTOR in aging, metabolism, and cancer. *Curr. Opin. Genet. Dev.* **23**, 53–62 (2013).

2. G. Y. Liu, D. M. Sabatini, mTOR at the nexus of nutrition, growth, ageing and disease. *Nat. Rev. Mol. Cell Biol.* **21**, 183–203 (2020).

3. H. Yang, D. G. Rudge, J. D. Koos, B. Vaidialingam, H. J. Yang, N. P. Pavletich, mTOR kinase structure, mechanism and regulation. *Nature* **497**, 217–223 (2013).

4. H. Yang, X. Jiang, B. Li, H. J. Yang, M. Miller, A. Yang, A. Dhar, N. P. Pavletich, Mechanisms of mTORC1 activation by RHEB and inhibition by PRAS40. *Nature* **552**, 368–373 (2017).

5. S. Wullschleger, R. Loewith, M. N. Hall, TOR signaling in growth and metabolism. *Cell* **124**, 471–484 (2006).

6. R. A. Saxton, D. M. Sabatini, mTOR signaling in growth, metabolism, and disease. *Cell* **168**, 960–976 (2017).

7. E. Kim, P. Goraksha-Hicks, L. Li, T. P. Neufeld, K.-L. Guan, Regulation of TORC1 by Rag GTPases in nutrient response. *Nat. Cell Biol.* **10**, 935–945 (2008).

8. Y. Sancak, T. R. Peterson, Y. D. Shaul, R. A. Lindquist, C. C. Thoreen, L. Bar-Peled, D. M. Sabatini, The rag GTPases bind raptor and mediate amino acid signaling to mTORC1. *Science* **320**, 1496–1501 (2008).

9. L. Bar-Peled, L. D. Schweitzer, R. Zoncu, D. M. Sabatini, Ragulator is a GEF for the Rag GTPases that signal amino acid levels to mTORC1. *Cell* **150**, 1196–1208 (2012).

10. M. Anandapadamanaban, G. R. Masson, O. Perisic, A. Berndt, J. Kaufman, C. M. Johnson, B. Santhanam, K. B. Rogala, D. M. Sabatini, R. L. Williams, Architecture of human Rag GTPase heterodimers and their complex with mTORC1. *Science* **366**, 203–210 (2019).

11. K. B. Rogala, X. Gu, J. F. Kedir, M. Abu-Remaileh, L. F. Bianchi, A. M. S. Bottino, R. Dueholm, A. Niehaus, D. Overwijn, A. P. Fils, S. X. Zhou, D. Leary, N. N. Laqtom, E. J. Brignole, D. M. Sabatini, Structural basis for the docking of mTORC1 on the lysosomal surface. *Science* **366**, 468–475 (2019).

12. M. Laplante, D. M. Sabatini, mTOR signaling in growth control and disease. *Cell* **149**, 274–293 (2012).

13. L. Bar-Peled, L. Chantranupong, A. D. Cherniack, W. W. Chen, K. A. Ottina, B. C. Grabiner, E. D. Spear, S. L. Carter, M. Meyerson, D. M. Sabatini, A tumor suppressor complex with GAP activity for the Rag GTPases that signal amino acid sufficiency to mTORC1. *Science* **340**, 1100–1106 (2013).

14. K. Shen, R. K. Huang, E. J. Brignole, K. J. Condon, M. L. Valenstein, L. Chantranupong, A. Bomaliyamu, A. Choe, C. Hong, Z. Yu, D. M. Sabatini, Architecture of the human GATOR1 and GATOR1-Rag GTPases complexes. *Nature* **556**, 64–69 (2018).

15. R. L. Wolfson, L. Chantranupong, G. A. Wyant, X. Gu, J. M. Orozco, K. Shen, K. J. Condon, S. Petri, J. Kedir, S. M. Scaria, M. Abu-Remaileh, W. N. Frankel, D. M. Sabatini, KICSTOR recruits GATOR1 to the lysosome and is necessary for nutrients to regulate mTORC1. *Nature* **543**, 438–442 (2017).

16. M. Peng, N. Yin, M. O. Li, SZT2 dictates GATOR control of mTORC1 signalling. *Nature* **543**, 433–437 (2017).

17. M. Peng, N. Yin, M. O. Li, Sestrins function as guanine nucleotide dissociation inhibitors for Rag GTPases to control mTORC1 signaling. *Cell* **159**, 122–133 (2014).

18. R. L. Wolfson, L. Chantranupong, R. A. Saxton, K. Shen, S. M. Scaria, J. R. Cantor, D. M. Sabatini, Sestrin2 is a leucine sensor for the mTORC1 pathway. *Science* **351**, 43–48 (2016).

19. L. Chantranupong, S. M. Scaria, R. A. Saxton, M. P. Gygi, K. Shen, G. A. Wyant, T. Wang, J. W. Harper, S. P. Gygi, D. M. Sabatini, The CASTOR proteins are arginine sensors for the mTORC1 pathway. *Cell* **165**, 153–164 (2016).

20. J. Chen, Y. Ou, R. Luo, J. Wang, D. Wang, J. Guan, Y. Li, P. Xia, P. R. Chen, Y. Liu, SAR1B senses leucine levels to regulate mTORC1 signalling. *Nature* **596**, 281–284 (2021).

21. D. Meng, Q. Yang, H. Wang, C. H. Melick, R. Navlani, A. R. Frank, J. L. Jewell, Glutamine and asparagine activate mTORC1 independently of Rag GTPases. *J. Biol. Chem.* **295**, 2890–2899 (2020).

22. X. Gu, J. M. Orozco, R. A. Saxton, K. J. Condon, G. Y. Liu, P. A. Krawczyk, S. M. Scaria, J. W. Harper, S. P. Gygi, D. M. Sabatini, SAMTOR is an *S*-adenosylmethionine sensor for the mTORC1 pathway. *Science* **358**, 813–818 (2017).

23. S. C. Lu, J. M. Mato, *S*-Adenosylmethionine in liver health, injury, and cancer. *Physiol. Rev.* **92**, 1515–1542 (2012).

24. S. Cai, Q. Ye, X. Zeng, G. Yang, C. Ye, M. Chen, H. Yu, Y. Wang, G. Wang, S. Huang, S. Quan, X. Zeng, S. Qiao, CBS and MAT2A improve methionine-mediated DNA synthesis through SAMTOR/mTORC1/S6K1/CAD pathway during embryo implantation. *Cell Prolif.* **54**, e12950 (2020).

25. J. L. Martin, F. M. McMillan, SAM (dependent) I AM: The *S*-adenosylmethionine-dependent methyltransferase fold. *Curr. Opin. Struct. Biol.* **12**, 783–793 (2002).

26. X. Cheng, S. Kumar, J. Posfai, J. W. Pflugrath, R. J. Roberts, Crystal structure of the HhaI DNA methyltransferase complexed with *S*-adenosyl-L-methionine. *Cell* **74**, 299–307 (1993).

27. H. L. Schubert, R. M. Blumenthal, X. Cheng, Many paths to methyltransfer: A chronicle of convergence. *Trends Biochem. Sci.* **28**, 329–335 (2003).

28. G. Yachdav, E. Kloppmann, L. Kajan, M. Hecht, T. Goldberg, T. Hamp, P. Honigschmid, A. Schafferhans, M. Roos, M. Bernhofer, L. Richter, H. Ashkenazy, M. Punta, A. Schlessinger, Y. Bromberg, R. Schneider, G. Vriend, C. Sander, N. Ben-Tal, B. Rost, PredictProtein—An open resource for online prediction of protein structural and functional features. *Nucleic Acids Res.* **42**, W337–W343 (2014).

29. A. Murayama, K. Ohmori, A. Fujimura, H. Minami, K. Yasuzawa-Tanaka, T. Kuroda, S. Oie, H. Daitoku, M. Okuwaki, K. Nagata, A. Fukamizu, K. Kimura, T. Shimizu, J. Yanagisawa, Epigenetic control of rDNA loci in response to intracellular energy status. *Cell* **133**, 627–639 (2008).

30. O. Cakici, M. Sikorski, T. Stepkowski, G. Bujacz, M. Jaskolski, Crystal structures of NodS *N*-methyltransferase from *Bradyrhizobium japonicum* in ligand-free form and as SAH complex. *J. Mol. Biol.* **404**, 874–889 (2010).

31. P. Z. Kozbial, A. R. Mushegian, Natural history of *S*-adenosylmethionine-binding proteins. *BMC Struct. Biol.* **5**, 19 (2005).

32. D. K. Liscombe, G. V. Louie, J. P. Noel, Architectures, mechanisms and molecular evolution of natural product methyltransferases. *Nat. Prod. Rep.* **29**, 1238–1250 (2012).

33. K. Tunyasuvunakool, J. Adler, Z. Wu, T. Green, M. Zielinski, A. Zidek, A. Bridgland, A. Cowie, C. Meyer, A. Laydon, S. Velankar, G. J. Kleywegt, A. Bateman, R. Evans, A. Pritzel, M. Figurnov, O. Ronneberger, R. Bates, S. A. A. Kohl, A. Potapenko, A. J. Ballard, B. Romera-Paredes, S. Nikolov, R. Jain, E. Clancy, D. Reiman, S. Petersen, A. W. Senior, K. Kavukcuoglu, E. Birney, P. Kohli, J. Jumper, D. Hassabis, Highly accurate protein structure prediction for the human proteome. *Nature* **596**, 590–596 (2021).

34. L. Holm, DALI and the persistence of protein shape. *Protein Sci.* **29**, 128–140 (2020).

35. X. Chen, X. Wang, J. Feng, Y. Chen, Y. Fang, S. Zhao, A. Zhao, M. Zhang, L. Liu, Structural insights into the catalytic mechanism of *Synechocystis* magnesium protoporphyrin IX *O*-methyltransferase (ChlM). *J. Biol. Chem.* **289**, 25690–25698 (2014).

36. J. H. Lee, B. Bae, M. Kuemin, B. T. Circello, W. W. Metcalf, S. K. Nair, W. A. van der Donk, Characterization and structure of DhpI, a phosphonate *O*-methyltransferase involved in dehydrophos biosynthesis. *Proc. Natl. Acad. Sci. U.S.A.* **107**, 17557–17562 (2010).

37. L. Lauinger, P. Kaiser, Sensing and signaling of methionine metabolism. *Metabolites* **11**, 83 (2021).

38. N. Shyh-Chang, J. W. Locasale, C. A. Lyssiotis, Y. X. Zheng, R. Y. Teo, S. Ratanasirintrawoot, J. Zhang, T. Onder, J. J. Unternaehrer, H. Zhu, J. M. Asara, G. Q. Daley, L. C. Cantley, Influence of threonine metabolism on *S*-adenosylmethionine and histone methylation. *Science* **339**, 222–226 (2013).

39. Y. J. Zhang, H. Yu, J. Zhang, H. Gao, S. Y. Wang, S. X. Li, P. Wei, J. Liang, G. Z. Yu, X. J. Wang, X. X. Li, D. W. Li, W. W. Yang, Cul4A-DDB1-mediated monoubiquitination of phosphoglycerate dehydrogenase promotes colorectal cancer metastasis via increased *S*-adenosylmethionine. *J. Clin. Investig.* **131**, e146187 (2021).

40. M. Kim, Y. Rho, R. Park, J. Y. Jung, G. S. Hwang, Y. K. Seo, J. H. Seo, Y. Heo, T. K. Ha, E. Ha, Duodenal-jejunal bypass maintains hepatic *S*-adenosylmethionine/*S*-homocysteine ratio in diet-induced obese rats. *Surg. Obes. Relat. Dis.* **17**, 1359–1368 (2021).

41. J. R. Barber, B. H. Morimoto, L. S. Brunauer, S. Clarke, Metabolism of *S*-adenosyl-L-methionine in intact human erythrocytes. *Biochim. Biophys. Acta* **886**, 361–372 (1986).

42. Z. Gai, Q. Wang, C. Yang, L. Wang, W. Deng, G. Wu, Structural mechanism for the arginine sensing and regulation of CASTOR1 in the mTORC1 signaling pathway. *Cell Discov.* **2**, 16051 (2016).

43. R. A. Saxton, L. Chantranupong, K. E. Knockenhauer, T. U. Schwartz, D. M. Sabatini, Mechanism of arginine sensing by CASTOR1 upstream of mTORC1. *Nature* **536**, 229–233 (2016).

44. J. Xia, R. Wang, T. Zhang, J. Ding, Structural insight into the arginine-binding specificity of CASTOR1 in amino acid-dependent mTORC1 signaling. *Cell Discov.* **2**, 16035 (2016).

45. A. V. Budanov, A. A. Sablina, E. Feinstein, E. V. Koonin, P. M. Chumakov, Regeneration of peroxiredoxins by p53-regulated sestrins, homologs of bacterial AhpD. *Science* **304**, 596–600 (2004).

46. R. A. Saxton, K. E. Knockenhauer, R. L. Wolfson, L. Chantranupong, M. E. Pacold, T. Wang, T. U. Schwartz, D. M. Sabatini, Structural basis for leucine sensing by the Sestrin2-mTORC1 pathway. *Science* **351**, 53–58 (2016).

47. S. Sharma, P. Watzinger, P. Kotter, K. D. Entian, Identification of a novel methyltransferase, Bmt2, responsible for the *N*-1-methyl-adenosine base modification of 25*S* rRNA in *Saccharomyces cerevisiae*. *Nucleic Acids Res.* **41**, 5428–5443 (2013).

48. Y. Huang, L. Ji, Q. Huang, D. G. Vassylyev, X. Chen, J. B. Ma, Structural insights into mechanisms of the small RNA methyltransferase HEN1. *Nature* **461**, 823–827 (2009).

49. Y. Yang, C. D. Eichhorn, Y. Wang, D. Cascio, J. Feigon, Structural basis of 7SK RNA 5′-'-gamma-pho methylation and retention by MePCE. *Nat. Chem. Biol.* **15**, 132–140 (2019).

50. W. Zhang, J. Tang, S. Wang, Z. Wang, W. Qin, J. He, The protein complex crystallography beamline (BL19U1) at the Shanghai synchrotron radiation facility. *Nucl. Sci. Tech.* **30**, 170 (2019).

51. W. Kabsch, XDS. *Acta Crystallogr.* **66**, 125–132 (2010).

52. M. Strong, M. R. Sawaya, S. Wang, M. Phillips, D. Cascio, D. Eisenberg, Toward the structural genomics of complexes: Crystal structure of a PE/PPE protein complex from *Mycobacterium tuberculosis*. *Proc. Natl. Acad. Sci. U.S.A.* **103**, 8060–8065 (2006).

53. I. J. Tickle, C. Flensburg, P. Keller, W. Paciorek, A. Sharff, C. Vonrhein, G. Bricogne, STARANISO (Global Phasing Ltd., 2018); http://staraniso.globalphasing.org/cgi-bin/staraniso.cgi.

54. P. D. Adams, P. V. Afonine, G. Bunkoczi, V. B. Chen, I. W. Davis, N. Echols, J. J. Headd, L. W. Hung, G. J. Kapral, R. W. Grosse-Kunstleve, A. J. McCoy, N. W. Moriarty, R. Oeffner, R. J. Read, D. C. Richardson, J. S. Richardson, T. C. Terwilliger, P. H. Zwart, PHENIX: A comprehensive Python-based system for macromolecular structure solution. *Acta Crystallogr.* **66**, 213–221 (2010).

55. P. Emsley, K. Cowtan, Coot: Model-building tools for molecular graphics. *Acta Crystallogr.* **60**, 2126–2132 (2004).

56. G. N. Murshudov, P. Skubak, A. A. Lebedev, N. S. Pannu, R. A. Steiner, R. A. Nicholls, M. D. Winn, F. Long, A. A. Vagin, REFMAC5 for the refinement of macromolecular crystal structures. *Acta Crystallogr.* **67**, 355–367 (2011).

57. Schrödinger, LLC, The PyMOL molecular graphics system, version 2.0 Schrödinger, LLC (2015).

58. P. Gouet, E. Courcelle, D. I. Stuart, F. Metoz, ESPript: Analysis of multiple sequence alignments in PostScript. *Bioinformatics* **15**, 305–308 (1999).

59. J. Vidgren, L. A. Svensson, A. Liljas, Crystal structure of catechol *O*-methyltransferase. *Nature* **368**, 354–358 (1994).